Low-repetition rate femtosecond laser writing of optical waveguides in KTP crystals: analysis of anisotropic refractive index changes

Muhammad Ali Butt,[1] Huu-Dat Nguyen,[1] Airán Ródenas,[1,*] Carolina Romero,[2] Pablo Moreno,[2] Javier R. Vázquez de Aldana,[2] Magdalena Aguiló,[1] Rosa Maria Solé,[1] Maria Cinta Pujol,[1] and Francesc Díaz[1]

[1]*Física i Cristal·lografia de Materials i nanomaterials (FiCMA-FiCNA), Universitat Rovira i Virgili (URV), 43007, Tarragona, Spain*

[2]*Laser Microprocessing Group, Facultad de Ciencias, Universidad de Salamanca, 37008 Salamanca, Spain*

[*]*airan.rodenas@urv.cat*

Abstract: We report on the direct low-repetition rate femtosecond pulse laser microfabrication of optical waveguides in KTP crystals and the characterization of refractive index changes after the thermal annealing of the sample, with the focus on studying the potential for direct laser fabricating Mach-Zehnder optical modulators. We have fabricated square cladding waveguides by means of stacking damage tracks, and found that the refractive index decrease is large for vertically polarized light (c-axis; TM polarized) but rather weak for horizontally polarized light (a-axis; TE polarized), this leading to good near-infrared light confinement for TM modes but poor for TE modes. However, after performing a sample thermal annealing we have found that the thermal process enables a refractive index increment of around $1.5\text{x}10^{-3}$ for TE polarized light, while maintaining the negative index change of around $-1\text{x}10^{-2}$ for TM polarized light. In order to evaluate the local refractive index changes we have followed a multistep procedure: We have first characterized the waveguide cross-sections by means of Raman micro-mapping to access the lattice micro-modifications and their spatial extent. Secondly we have modeled the waveguides following the modified region sizes obtained by micro-Raman with finite element method software to obtain a best match between the experimental propagation modes and the simulated ones. Furthermore we also report the fabrication of Mach-Zehnder structures and the evaluation of propagation losses.

OCIS codes: (160.1190) Anisotropic optical materials; (230.7370) Waveguides.

References and links

1. G. M. Loiacono, D. N. Loiacono, and R. A. Stolzenberger, "Growth and properties of crystals in the system $KTiOPO_4$-$NaTiOPO_4$," J. Cryst. Growth **144**(3-4), 223–228 (1994).
2. P. Yankov, D. Schumov, A. Nenov, and A. Monev, "Laser damage tests of large flux-grown $KTiOPO_4$ crystals," Opt. Lett. **18**(21), 1771–1773 (1993).
3. M. E. Hagerman and K. R. Poeppelmeier, "Review of the structure and processing-defect-property relationships of Potassium Titanyl Phosphate: a strategy for novel thin-film photonic devices," Chem. Mater. **7**(4), 602–621 (1995).
4. J. D. Bierlein, A. Ferretti, L. H. Brixner, and W. Y. Hsu, "Fabrication and characterization of optical waveguides in $KTiOPO_4$," Appl. Phys. Lett. **50**(18), 1216–1218 (1987).
5. F. Laurell, J. B. Brown, and J. D. Bierlein, "Sum- frequency generation in segmented KTP waveguides," Appl. Phys. Lett. **60**(9), 1064–1066 (1992).
6. M. Rusu, E. U. Rafailov, R. Herda, O. G. Okhotnikov, S. M. Saltiel, P. Battle, S. McNeil, A. B. Grudinin, and W. Sibbett, "Efficient generation of green and UV light in a single PP-KTP waveguide pumped by a compact all-fiber system," Appl. Phys. Lett. **88**(12), 121105 (2006).

#237800 - $15.00 USD Received 10 Apr 2015; revised 22 May 2015; accepted 25 May 2015; published 2 Jun 2015

7. K. A. Fedorova, M. A. Cataluna, P. R. Battle, C. M. Kaleva, I. L. Krestnikov, D. A. Livshits, and E. U. Rafailov, "Orange light generation from a PPKTP waveguide end pumped by a CW quantum-dot tunable laser diode," Appl. Phys. B **103**(1), 41–43 (2011).
8. F. Laurell, "Periodically poled materials for miniature light sources," Opt. Mater. **11**(2-3), 235–244 (1999).
9. Y. Cheng, J. Yuechen, A. Shavkat, S. Zhou, and F. Chen, "Guided-wave phase-matched second-harmonic generation in $KTiOPO_4$ waveguide produced by swift heavy-ion irradiation," Opt. Eng. **53**(11), 117102 (2014).
10. Y. F. Zhou, P. Liu, T. Liu, L. Zhang, X. F. Yu, T. J. Wang, J. H. Zhao, and X. L. Wang, "Visible and near-infrared optical properties of a proton-implanted KTP waveguide," Appl. Opt. **53**(21), 4779–4783 (2014).
11. F. Schrempel, T. Höche, J. P. Ruske, U. Grusemann, and W. Wesch, "Depth dependence of radiation damage in Li^+-implanted $KTiOPO_4$," Nucl. Instrum. Methods Phys. Res. B **191**(1–4), 202–207 (2002).
12. K. M. Wang, B. R. Shi, N. Cue, Y. Y. Zhu, R. F. Xiao, F. Lu, W. Li, and Y. G. Liu, "Waveguide laser film in erbium-doped $KTiOPO_4$ by pulsed laser deposition," Appl. Phys. Lett. **73**(8), 1020–1022 (1998).
13. F. Schrempel, T. Opfermann, J. P. Ruske, U. Grusemann, and W. Wesch, "Properties of buried waveguides produced by He-irradiation in KTP and Rb:KTP," Nucl. Instrum. Methods Phys. Res. B **218**, 209–216 (2004).
14. S. Campbell, R. R. Thomson, D. P. Hand, A. K. Kar, D. T. Reid, C. Canalias, V. Pasiskevicius, and F. Laurell, "Frequency-doubling in femtosecond laser inscribed periodically-poled potassium titanyl phosphate waveguides," Opt. Express **15**(25), 17146–17150 (2007).
15. S. Zhang, J. Yao, W. Liu, Z. Huang, J. Wang, Y. Li, C. Tu, and F. Lu, "Second harmonic generation of periodically poled potassium titanyl phosphate waveguide using femtosecond laser pulses," Opt. Express **16**(18), 14180–14185 (2008).
16. S. Müller, T. Calmano, P. W. Metz, C. Kränkel, C. Canalias, C. Liljestrand, F. Laurell, and G. Huber, "Highly efficient continuous wave blue second-harmonic generation in fs-laser written periodically poled Rb:$KTiOPO_4$ waveguides," Opt. Lett. **39**(5), 1274–1277 (2014).
17. F. Laurell, T. Calmano, S. Müller, P. Zeil, C. Canalias, and G. Huber, "Laser-written waveguides in KTP for broadband Type II second harmonic generation," Opt. Express **20**(20), 22308–22313 (2012).
18. N. Dong, F. Chen, and J. R. Vázquez de Aldana, "Efficient second harmonic generation by birefringent phase matching in femtosecond-laser-inscribed KTP cladding waveguides," Phys. Status Solidi RLL **6**(7), 306–308 (2012).
19. N. Dong, Y. Tan, A. Benayas, J. V. de Aldana, D. Jaque, C. Romero, F. Chen, and Q. Lu, "Femtosecond laser writing of multifunctional optical waveguides in a Nd:YVO_4 + KTP hybrid system," Opt. Lett. **36**(6), 975–977 (2011).
20. R. Solé, V. Nikolov, I. Koseva, P. Peshev, X. Ruiz, C. Zaldo, M. J. Martín, M. Aguiló, and F. Díaz, "Conditions and possibilities for rare-earth doping of $KTiOPO_4$ flux-grown single crystals," Chem. Mater. **9**(12), 2745–2749 (1997).
21. K. Iliev, P. Peshev, V. Nikolov, and I. Koseva, "Physicochemical properties of high-temperature solutions of the K_2O-P_2O_5-TiO_2 system suitable for the growth of $KTiOPO_4$ (KTP) single crystals," J. Cryst. Growth **100**(1), 219–224 (1990).
22. K. Kato and E. Takaoka, "Sellmeier and thermo-optic dispersion formulas for KTP," Appl. Opt. **41**(24), 5040–5044 (2002).
23. Y. Tsuji and M. Koshiba, "Guided-Mode and Leaky-Mode analysis by imaginary distance beam propagation method based on Finite Element scheme," J. Lightwave Technol. **18**(4), 618–623 (2000).
24. H. Karakuzu, M. Dubov, and S. Boscolo, "Control of the properties of micro-structured waveguides in lithium niobate crystal," Opt. Express **21**(14), 17122–17130 (2013).
25. A. Ródenas, G. A. Torchia, G. Lifante, E. Cantelar, J. Lamela, F. Jaque, L. Roso, and D. Jaque, "Refractive index change mechanisms in femtosecond laser written ceramic Nd: YAG waveguides: micro-spectroscopy experiments and beam propagation calculations," Appl. Phys. B **95**(1), 85–96 (2009).
26. A. Ródenas, L. M. Maestro, M. O. Ramírez, G. A. Torchia, L. Roso, F. Chen, and D. Jaque, "Anisotropic lattice changes in femtosecond laser inscribed Nd^{3+}: MgO: $LiNbO_3$ optical waveguides," J. Appl. Phys. **106**(1), 013110 (2009).
27. G. E. Kugel, F. Brehat, B. Wyncke, M. D. Fontana, G. Marnier, C. Carabatos-Nedelec, and J. Mangin, "The vibrational spectrum of a $KTiOPO_4$ single crystal studied by Raman and infrared reflectivity spectroscopy," J. Phys. C Solid State Phys. **21**(32), 5565–5583 (1988).

1. Introduction

Potassium titanyl phosphate ($KTiOPO_4$, hereafter, KTP) and its isostructurals are well known for their excellent physical properties. KTP is a well-known acentric non-linear optical (NLO) material, belonging to the space group $Pna2_1$ with unit cell parameters a = 12.818(Å), b = 6.404(Å) and c = 10.590(Å) [1]. As a NLO crystal, it possesses a high laser damage threshold (around 3 GW/cm^2 at 1064 nm [2]) and also large non-linear and electro-optic coefficients [3]. It also offers broad thermal and angular acceptance angle for second harmonic generation. In fact, KTP is largely used for doubling the 1064 nm Nd:YAG radiation and offers exceptional versatility for device design in both the bulk and epitaxial layer.

#237800 - $15.00 USD Received 10 Apr 2015; revised 22 May 2015; accepted 25 May 2015; published 2 Jun 2015

As an interesting material, waveguides fabrication in this host has been done from the 1987, traditionally by ion-exchange methods [4]. Already by periodically poling the waveguides, these Quasi Phase Matched (QPM) KTP waveguides have been used to generate coherent blue light [5,6], and also orange [7]. However, the ion-exchange waveguides in KTP suffer from degradation with the time when submitted to high visible powers problems with the reproducibility due to the dependence of the ion-exchange rate with the vacancy concentration which changes from crystal to crystal and also by the crystal growth method [8]. More recently, waveguides in KTP have been fabricated by ion irradiation [9] and proton implantation [10], but some partial lattice damage can be created. Other methods have been used to fabricate one waveguides in KTP such as ion implantation [11] and pulsed laser deposition [12]. Buried channel waveguides were also fabricated by multiple He^+ ion implantations [13].

The use of the direct laser writing (DLW) technique allows to microfabricate three-dimensional (3D) guiding devices capable of unprecedented light control functions, when compared to other surface microfabrication techniques. Previous works in DLW waveguides in KTP crystals have focused on evaluating the potential for achieving high efficiency waveguided second harmonic generation (SHG) both by means of periodically poling the crystal to achieve quasi-phase matching (QPM) [14–16], or by performing Type II ($e^{\omega} + o^{\omega} \rightarrow e^{2\omega}$) around 1 micron→ green PM SHG [17, 18] and also, in an Nd:YVO_4 + KTP hybrid system to obtain multifrequency waveguide lasers [19]. Instead we have focused on studying the potential for direct laser fabricating Mach-Zehnder optical modulators (M-Z) in KTP crystals for operation at 1.55 μm telecom wavelength. We report the first steps towards achieving efficient M-Z devices for use at 1.5 μm wavelength.

2. Experimental and technical details

2.1. Crystal growth and preparation

For this work we used Na doped KTP samples available in our laboratory from previous works. Na:KTP single crystals were grown from high temperature solution (HTS) by using Top Seeded Solution Growth technique by slow cooling (TSSG-SC). HTS are used for growing crystals with incongruent melting and in the case with polymorphic transitions before melting. High quality large single crystals of KTP family can be grown by this technique in a single-zone furnace [20]. The reagents used were K_2CO_3, TiO_2, $NH_4H_2PO_4$, Na_2CO_3 and WO_3 with a purity levels of 99.9%. In order to decrease the viscosity of the solution for easier homogenization and mixing of the solution, we have used 30 mol% of WO_3. The solution composition used was K_2O-Na_2O-TiO_2-P_2O_5-WO_3 = 37.8-4.2-14-14-30 (mol %), taking into account the crystallization region for KTP in the ternary system [21]. For these experiments, we have used a platinum cylindrical crucible of 100 cm^3 filled with 150 g of solution and homogenized at 50-60 K above the expected saturation temperature for 6-7 h. The saturation temperature of this solution, which was carefully determined by repeated seeding, is around 1221 K. The seed oriented along c crystallographic direction was used because in previous works [20] it has been proved that the crystals grow with high crystalline quality with this orientation and these crystals are with enough size for cutting several substrates perpendicular to ***c*** crystallographic direction.

The vertical thermal gradient in the solution was 3.8 K/cm. After determining the saturation temperature of the solution, a cooling rate of 0.1 K/h was applied for 15 K and 0.05 K/h for the next 11-14 K. The seed rotation was maintained at 60 rpm for few days and reduced gradually as the crystal grew. When the crystal was fully grown, it was slowly extracted from the solution and maintained slightly above the solution's surface while the furnace was cooled to room temperature at a typical rate of 30-40 K/h. The slow cooling process of the system prevents the crystal from cracking due to thermal shocks. As a result, high quality crystals with dimensions around 12 x 23 x 12.5 mm^3 were obtained. After that

#237800 - $15.00 USD Received 10 Apr 2015; revised 22 May 2015; accepted 25 May 2015; published 2 Jun 2015

cutting and polishing of the crystal used in this work was performed by Minitom Struers diamond disk saw and polishing suspension SF1 from Logitech Company, respectively. The crystal composition measured by Electron probe microanalysis was $K_{0.97}Na_{0.03}TiOPO_4$.

2.2 Direct laser writing of waveguide structures

The waveguides fabricated in this paper consist on square cladding structures performed by means of 3D-DLW. Cladding waveguides allow to propagate light inside the so called cladding region thanks a decreased index of refraction which acts as an optical potential barrier which supports a localized leaky mode. The difficulty in controlling this type of waveguides resides in achieving the desired mode properties (number of modes, mode effective index, and mode field diameters). Cladding waveguides were fabricated using a Ti:Sapphire regenerative amplifier laser system (Spitfire and Tsunami systems, Spectra-Physics) generating linearly polarized pulses of around 120 fs temporal pulse width, with a central wavelength of around 795 nm, and with a repetition rate of 1 kHz. The precise value of the pulse energy used to irradiate the sample was achieved using a calibrated neutral density filter, and a set of half-wave plate and linear polarizer. The beam was focused through the (001) crystal plane along the ***c***-axis at a linear depth of 75 μm by a 20X microscope objective to produce damage filaments. Laser polarization was kept along the ***a***-axis.

In order to fabricate the waveguide claddings parallel scans (with 4 μm separation between adjacent scans) were done at different depths of the sample, following the desired geometry (square) that was programmed in the motorized stage. In order to avoid the shielding and distortion of the incident pulses, the structure was fabricated from large to small depth values. In this way, cladding waveguides with widths of 20, 30 and 40 μm were produced. In this paper we only report the results of 20 and 30 μm since bigger claddings resulted in too multimode waveguides with no use for interferometric applications. The scanning velocity and pulse energy were 700 μm/s and 0.6 μJ, respectively.

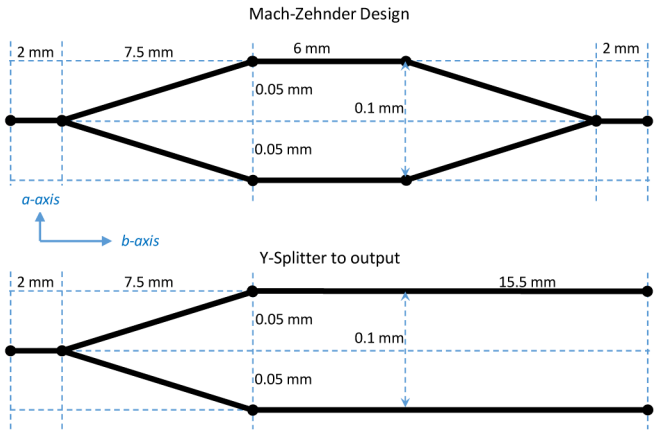

Fig. 1. Top: Mach-Zehnder designs. Bottom: Y-splitter designs.

Apart from straight waveguides, Mach-Zehnder structures were also fabricated to evaluate the extra losses imposed by waveguide splitting and joints. To simplify the fabrication, splitters were designed as simple Y-junctions with no bending. Figure 1 shows the schematic design followed for these structures: in the Mach-Zehnder structure, the input and output zones were left of 2 mm length, Y-junction lengths of 7.5 mm were used, and straight branches were of 4 mm. Splitters only were also fabricated to evaluate the output modes after splitting sections. It is important to remember that cladding waveguides fabricated by ultrashort pulse lasers always have residual stress and complex index distributions, and therefore the modal analysis can be more complex than that of step-index waveguides.

#237800 - $15.00 USD Received 10 Apr 2015; revised 22 May 2015; accepted 25 May 2015; published 2 Jun 2015

2.3 Optical waveguide characterization

Optical waveguides were characterized using a 1.52 μm wavelength HeNe laser and an optical bench with input and output focusing lenses with 5-axis microcontrollers. A quarter-wave plate was used to pre-convert the laser linear polarization into circular one, so that linear polarizers could then be used to evaluate the optical modes and losses for both TM (vertical) and TE (horizontal) orthogonal polarizations. For launching light into the waveguides an aspheric lens C430TME-C from Thorlabs was used, having a NA of 0.15. For output imaging a 20X Mitutoyo Plan Apo NIR Infinity-Corrected Objective was used, having a NA of 0.4. Mode images were obtained and recorded on a FLIR SC7000 IR camera. Power measurements were performed with a germanium OP-2 IR photodiode with 1 nW resolution and a LabMax-TOP meter from Coherent. Insertion losses were always obtained by measuring the output power of each waveguiding element and referring it to the same optical system output power without the waveguide element. A linear polarizer was always used before the input lens and after the output lens so that both polarized imaging and polarized power measurements were performed. Using this setup the input lens laser spot was measured to have a mode field diameter (MFD, measured at $1/e^2$ intensity level) of 8.55 μm for both TM and TE polarizations. A calibration target was used to obtain the camera field of view spatial extensions.

2.4. Sample annealing

A vertical furnace with temperature gradient near zero at the central part was used to perform the annealing of the fabricated waveguides. An initial heating ramp of 50 K/min was used until 673 K was achieved. The sample was left at this temperature in air for 1 hour, and a slow cooling with a rate of 1 K/h to room temperature was applied overnight.

2.5 Micro-Raman mapping

Confocal μ-Raman high-resolution cross-sectional mapping of the waveguide facets was performed using a Renishaw inVia Reflex microscope attached to a 514 nm argon laser. The Raman signal was obtained in a back-scattering configuration by using a filled 1.42NA oil immersion Olympus PLAPON 60XO microscope objective with an estimated focal diameter spot of ~435 nm at a $1/e^2$ intensity ($d_{spot} = 1.22\lambda_0/NA$), at 514 nm wavelength. The Raman spectra were obtained for ***a***-axis excitation polarization and un-polarized for detection. Incident and collected beam were travelling parallel to ***c***-axis. A 2400 lines/mm grating was used covering the range 300-800 cm^{-1}. Exposure times were of 1 second, raster scan spatial steps were of 400 nm, and total mapping area was of 100x100 μm^2. Total measuring time was of 23 h. Spectral analysis of data was performed using WiRE®3.4 software to deconvolute each measured spectra to obtain the different phonon mode components: energy, linewidth, and intensity. All 12 observed phonon modes were simultaneously fitted to Lorentzian shapes.

2.6 Mode simulation

The commercial simulation software COMSOL Multiphysics was used in our modeling. It is based on the finite element method (FEM) for approximating partial differential equations. The model was simulated using a designed geometry that matches the fabricated track-cladding structure after micro-Raman analysis. The simulated cladding consisted on 18 elliptical tracks (12 tracks on top and bottom, 6 track on the sides) forming a cladding structure. The inner core formed within the cladding is in a shape of rectangle 14x18 μm^2. The simulation was computed with wavelength of 1.52 μm corresponding to KTP refractive indices of $n_z = 1.8165$ and $n_x = 1.7287$ for TM and TE modes respectively [22]. In order to truncate the computational domain and reduce light reflection from the boundary, a perfectly matched layer (PML) was applied surrounding the cladding waveguide structure [23, 24]. The

#237800 - $15.00 USD Received 10 Apr 2015; revised 22 May 2015; accepted 25 May 2015; published 2 Jun 2015

PML was chosen as a circular layer which locates around the cladding structure and isotropic in its absorption.

3. Results

3.1 Crystalline substrates

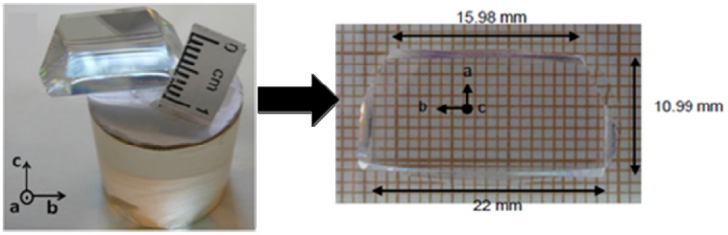

Fig. 2. Na:KTP bulk single crystal grown by TSSG-SC and a cut and polished Na:KTP(001) oriented substrate.

The waveguides fabrication was performed on the sample with dimensions of 11.0 x 22 x 1.6 mm^3 (along *a* x *b* x *c*, which are the X, Y and Z dielectric axes, respectively), and with a roughness of 22.8 nm and bent radius of 152.54 m. Figure 2 shows a photograph of the prepared sample before waveguide fabrication. The channels were fabricated parallel to the ***b*** crystallographic direction.

3.2 As-fabricated waveguide analysis

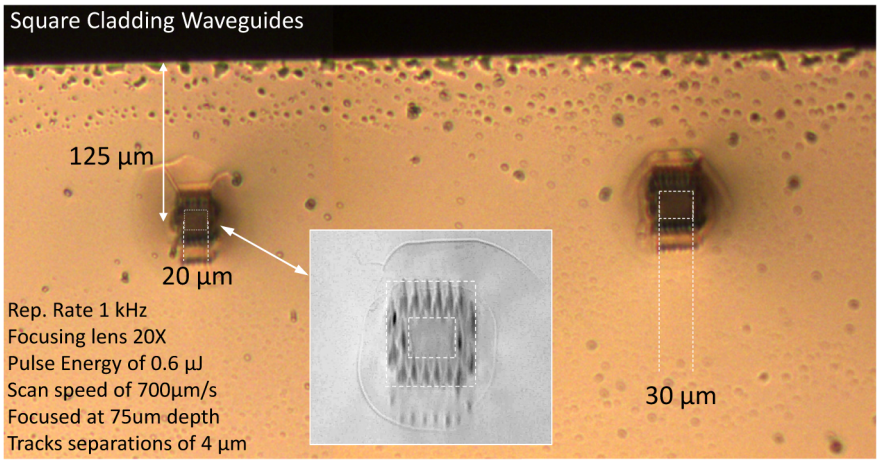

Fig. 3. Optical microscope picture of as-fabricated straight waveguides (SW) with cladding sizes of 20 µm (left) and 30 µm (right). Inset shows a higher resolution image where single tracks can be better distinguished.

All waveguides were first characterized in a bright field microscope after optical polishing, and before insertion in the optical guiding setup. Figure 3 shows an example of two straight cladding waveguides with widths of 20 µm and 30 µm. All M-Z and Y-splitters were fabricated with the same square cladding designs, only changing the required number of tracks. All central waveguide depths were measured to be of around 125 µm.

To evaluate the as-fabricated waveguides, optical mode characterization was performed at 1.52 µm wavelength for all straight waveguides (SW), Mach-Zehnders (M-Z) and Y-Splitters (Y-S). It was found that the 20 µm straight cladding waveguide (hereafter 20SW) guided TM light very well, but optical confinement for TE polarized light was very poor. The same

#237800 - $15.00 USD Received 10 Apr 2015; revised 22 May 2015; accepted 25 May 2015; published 2 Jun 2015

behavior was observed for the 30 μm width cladding waveguide (30SW). Figure 4 summarizes the observed modes for both TE (left) and TM (right) polarizations for both 20SW and 30SW, as well as for 20M-Z and 30M-Z. Input spots are also shown for comparison.

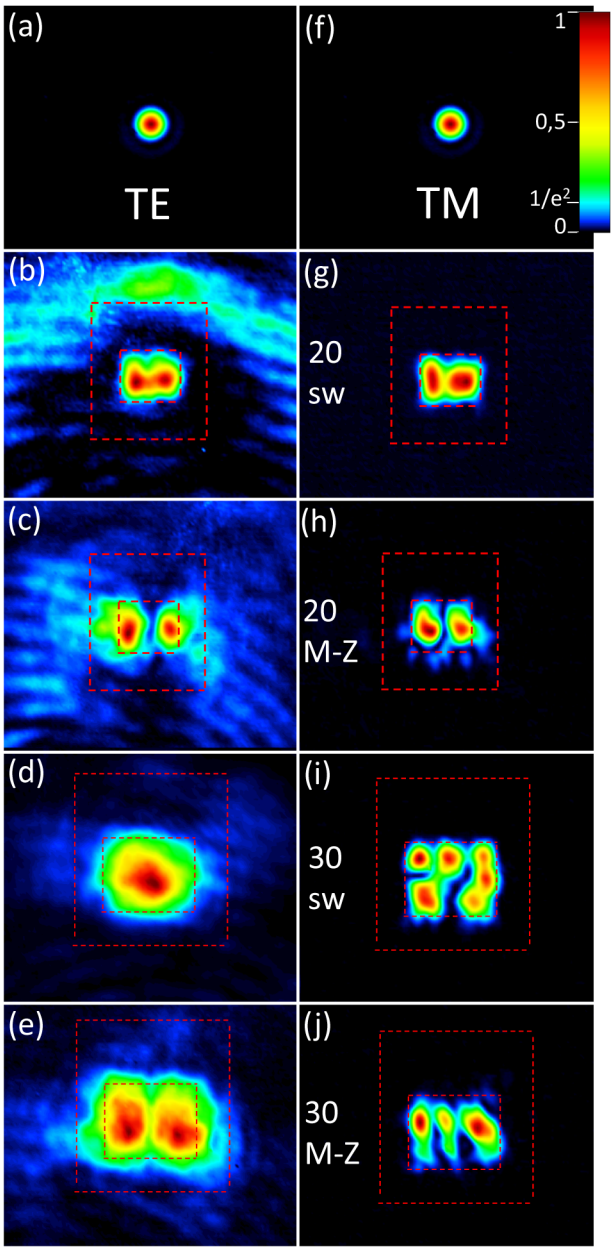

Fig. 4. (a) and (b) Recorded optical modes for input spots, (b), (g), (d) and (i) straight waveguides (20SW and 30SW) and (c), (h),(e), (j) also for Mach-Zehnders (20M-Z and 30M-Z). Left shows TE polarized modes and right shows TM polarized modes. Red dashed lines are guidelines for the fabricated claddings, as measured from optical micrographs.

As it can be observed from Figs. 4(b) and 4(c), the 20SW waveguide and 20M-Z confine very poorly TE polarized light, probably due to a very low index contrast of the fabricated

#237800 - $15.00 USD Received 10 Apr 2015; revised 22 May 2015; accepted 25 May 2015; published 2 Jun 2015

cladding. A large portion of light is seen to propagate outside the waveguide, which in the case of the M-Z is more exacerbated due to the y-splitting and joints, which spread light out of the cladding. In the case of the larger claddings 30SW and 30M-Z the effect is less remarked thanks to the thicker and larger cladding extension, but still a large amount of TE light was observed to propagate outside of the waveguide. In the case of TM polarized light the confinement was in contrast much better, this indicating a strong index decrease in the cladding volume, this creating a good mode localization with very low light leakage outside of the cladding volumes. Figures 4(g)-4(j) show that all structures are multimode at 1.52 µm wavelength. In the case of the M-Z structures, all outputs were observed to have an unclean field distribution due to the mode splitting and joints. It is important to note that the color scale used for the field intensities show the $1/e^2$ level in light blue, so that it can be clearly seen that all TM modes have an almost 100% power distribution well inside the cladding elements. This is in bright contrast to TE polarized light, where the modes always overlap with the cladding structures, therefore becoming very lossy. From this results it can be also preliminary concluded that in order to obtain a strictly single mode behavior for future M-Z devices, the cladding structures must keep the same vertical size as the 20SW, but its width should be reduced.

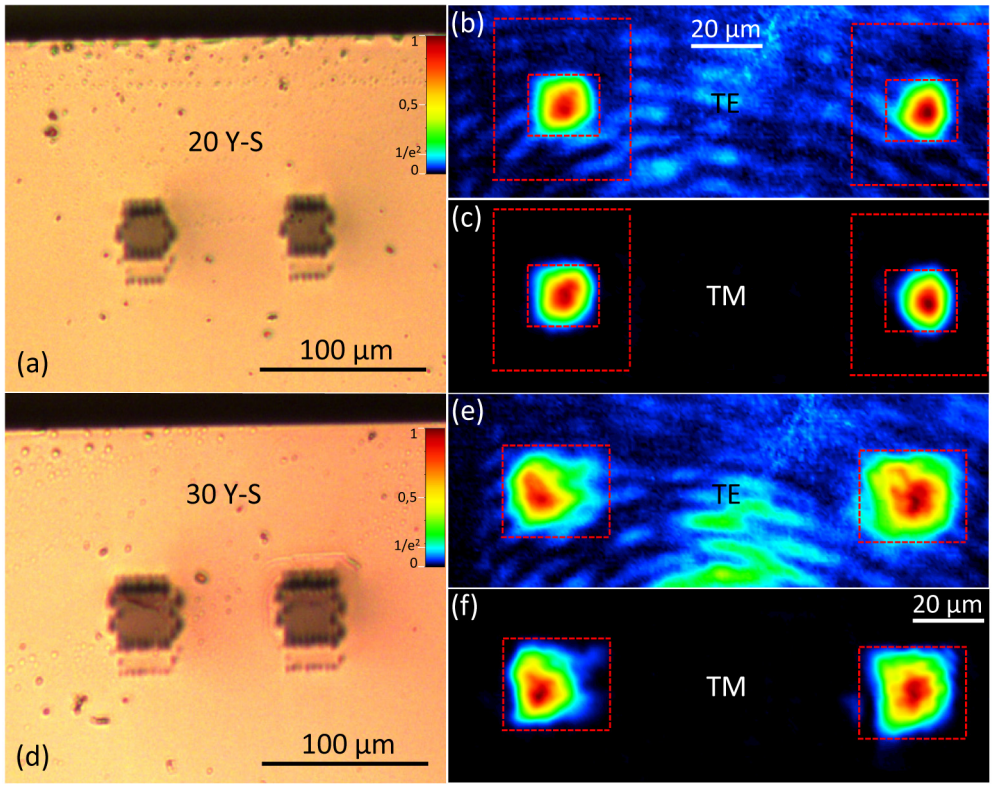

Fig. 5. Microscope pictures and output fundamental modes of both Y-Splitter 20Y-S and 30Y-S for both TE and TM polarizations.

In order to evaluate how the cladding waveguide split the modes in two, Y-splitters (Y-S) were also characterized in its output. Figures 5(a) and 5(d) shows the recorded micrographs of both 20Y-S and 30Y-S, as well as the fundamental modes obtained by careful alignment of the input beam relative position to the SW inputs. As it can be observed in Fig. 5, the as-fabricated waveguide structures do not confine TE light inside the cladding, whereas for TM polarized light the confinement is rather good as observed in Figs. 5(c) and 5(f). Note that

#237800 - $15.00 USD Received 10 Apr 2015; revised 22 May 2015; accepted 25 May 2015; published 2 Jun 2015

higher order modes were also observed, but are not shown here for the sake of brevity. As previously mentioned, to obtain a purely single mode behavior the 20 µm width claddings should be reduced to around half the width so that no higher orders could be supported.

3.3. Post-annealing waveguiding results

Direct laser written damage tracks are known to not only have a reduced index of refraction, but also produce strong stress fields around damage tracks and can yield to index change fields that are not purely depressed, but also to increased index zones due to the typical anisotropic index changes associated to stress fields [25,26]. In order to erase this stress [25] and to evaluate the changes in the waveguides modes, an annealing process was performed as detailed in the previous section §2.4. Figure 6 shows the compared results of output modes of 20SW before and after the annealing process.

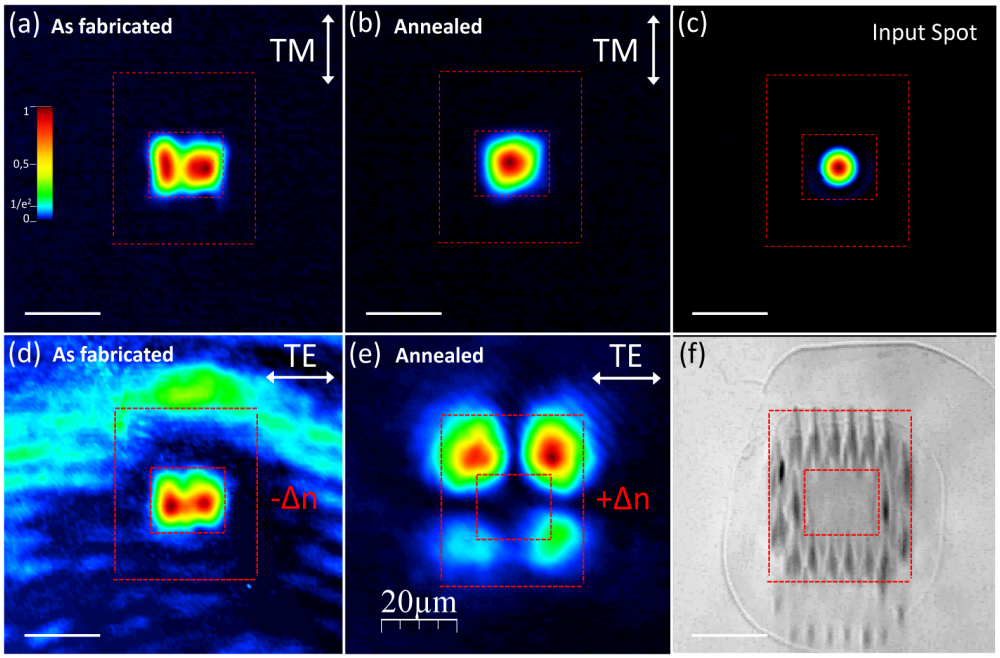

Fig. 6. (a) and b) TM modes before and after annealing respectively. (c) input spot for comparison. (d) and (e) TE modes before and after annealing respectively. (f) microscope picture of the 20SW. All dashed red lines are a guideline of the cladding area. Scale bar 20 µm.

As it is shown in Fig. 6, for TM polarized light a fundamental mode could be observed, although a higher order mode was also observed. The degree of mode confinement was not decreased, this indicates that the depressed cladding index profile for TM polarization was not deteriorated during the annealing process. Surprisingly, for TE polarization a very different behavior was observed: the depressed index profile changed to an increased profile where light propagation and mode confinement could be observed inside the laser written volumes. This is, to our knowledge, the first report of a laser written refractive index increase in KTP crystals. Figure 6 (e) shows one of the observed modes as example of the clear optical guiding inside the laser written region. Due to the fact that the written volume is very large, guiding could be observed to happen inside all the cladding regions, i.e. in the upper tracks row, and also in the lateral columns and lower track row. Since this effect is very unusual, and in order to understand the nature of the KTP lattice changes inside the cladding region, a two-dimensional micro-Raman mapping was performed all through the 20SW cross-section (see next section).

#237800 - $15.00 USD Received 10 Apr 2015; revised 22 May 2015; accepted 25 May 2015; published 2 Jun 2015

Table 1. Measured Losses for 20SW and 20M-Z structures

	Before annealing (TM)		**After annealing (TM)**	
	20SW	*20M-Z*	***20SW***	***20M-Z***
Insertion Loss (dB)	12.4	10.7	**7.3**	**5.8**
Prop. Loss (dB/cm)	4.4	-	**2.4**	**-**

In the case of the smallest waveguide cladding size of 20 μm losses were also evaluated (at 1.52 μm wavelength). Before annealing, the 20SW insertion losses were of 12.4 dB, and surprisingly for the 20M-Z these losses were reduced by almost 2 dB to 10.7 dB. This can be understood in terms of in-plane recapture of scattered light at the splitted branches and also at the combination section and this can also explain the fact that the M-Z output modes are always observed to have a more complex intensity spatial distribution. After annealing, an improvement of 5 dB was obtained for the insertion losses of 20SW which were of 7.3 dB, this implying reduced scattering losses probably due to two reasons: first a lower overlap between the excited modes and the cladding volume and secondly due to a reduced number of scattering defects after the annealing process. By performing a mode overlap function between the input lens mode, and the waveguide fundamental modes before and after the annealing, propagation losses could also be obtained by subtracting from the insertion losses the Fresnel losses at both sample facets and the input coupling losses. The propagation losses were estimated to be of 4.4 dB/cm before and of 2.4 dB/cm after the annealing process. For the 20M-Z the insertion losses were lower also after the annealing and of 5.8 dB, this implying that still the mentioned effects could be occurring. Since these waveguides are not single mode, and higher order modes have a larger interaction zone with the cladding volume which can cause light scattering, it is believed that a decrease of the horizontal cladding width so as to produce a single mode behavior could decrease the losses while allowing for the M-Z structures to be fabricated. Table 1 summarizes the losses measurements for 20SW and 20M-Z for TM polarization.

3.4. Micro-Raman analysis

Figure 7(a) shows three measured Raman spectra (see section §2.5 for details) corresponding to normal un-irradiated volume (black), to inside the tracks volumes (red), and to the bottom apex volumes of the tracks (blue). It can be observed that there is not much lattice breaking and distortion since both the Raman spectra intensities and shapes are well kept in all areas. A more detailed analysis, however, reveals that there are slight lattices distortions that can explain the previously observed anisotropic refractive index changes. Figure 7(c) shows the phonon peak full width at half maximum (FWHM) of the υ_1/υ_3 (TiO_6 octahedra) phonon mode at 693.7 cm^{-1} [27]. Almost all of the other phonon peaks showed qualitatively similar behavior in width, consisting of a clear broadening of around 2 cm^{-1}. This broadening is stronger at the upper row of tracks than at the lower row, and is well localized at each single track. Phonon broadening is characteristic of lattice distortion, indicating that the KTP crystalline lattice order has been slightly reduced at damage tracks as a result of lattice distortions and defect creation. Although not shown here for the sake of brevity, almost all phonon peaks also showed a general decrease in peak intensity and integrated area, also localized at the damage tracks. Similar tendency has been reported by Zhou *et al.* [10], they observed a general decrease in the raman peaks when comparing the proton-implanted region versus the non implanted region in a KTP waveguide. This also indicates that at these regions a higher density of crystalline lattice defects is present. As it is generally correct for most transparent crystalline dielectrics, a slight amorphization of the crystalline lattice is usually accompanied by a decrease in the index of refraction, which is consistent with the observed lower index of the cladding region.

#237800 - $15.00 USD Received 10 Apr 2015; revised 22 May 2015; accepted 25 May 2015; published 2 Jun 2015

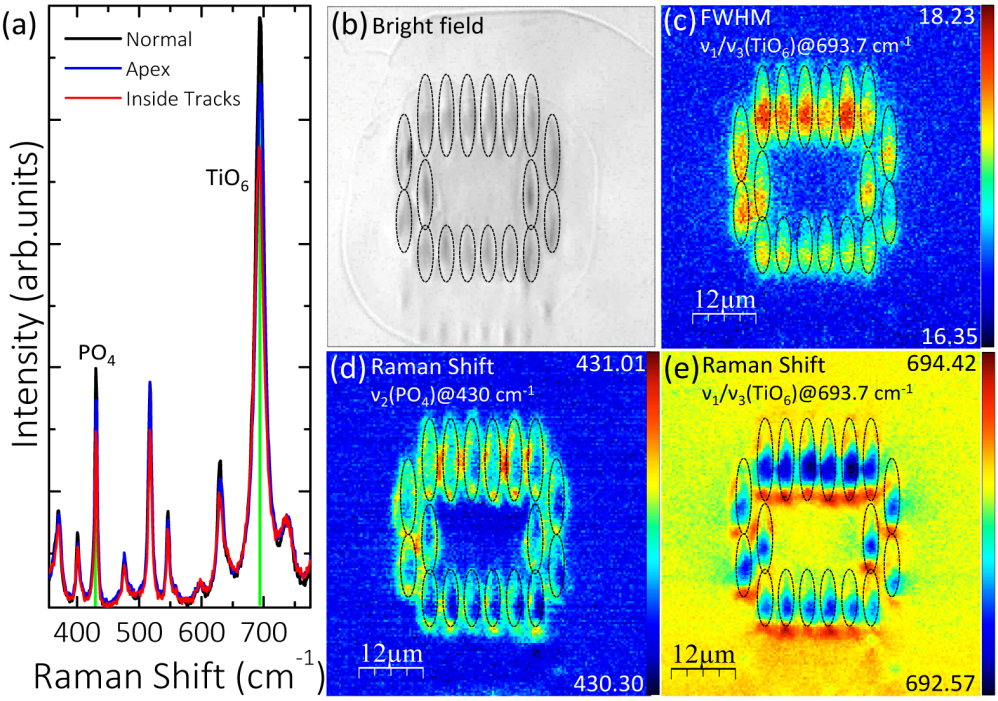

Fig. 7. (a) Raman spectra after annealing for un-irradiated volumes (black), track bottom apex volumes (blue) and inside tracks (red). (b) Micrograph of the 20SW. (c) Full width half maximum (FWHM) of the υ_1/υ_3 (TiO_6) phonon mode at 693.7 cm^{-1}. (d) Energy shift of the υ_2 (PO_4) phonon mode at 430 cm^{-1}. (d) Energy shift of the υ_1/υ_3 (TiO_6) phonon mode at 693.7 cm^{-1}. Dashed black lines indicating the track volumes have been sketched following the apparent size of tracks as seen from the overall Raman mapping results.

The energy shifts of the υ_1/υ_3 (TiO_6 octahedra) phonon mode at 693.7 cm^{-1} and of the υ_2 (PO_4 tetrahedra) phonon mode at 430 cm^{-1} also show (see Figs. 7(d) and 7(e)) that lattice distortions by anisotropic compressive and tensile stress has occurred inside the tracks. It is important to recall that this Raman analysis was performed after the as-fabricated sample was annealed, and therefore these lattice changes are the resulting crystalline state after the thermal relaxation process. For the υ_2 phonon mode (see Fig. 7(d)) a clear blue-shift of around + 0.57 cm^{-1} is observed in the tracks surroundings, therefore an anisotropic lattice distortion mostly distributed all across the cladding volume can be expected. Similarly, the υ_1/υ_3 phonon mode also shows marked energy shifts. However, in this case a more complex distribution is observed. Firstly, the interior of the damage tracks presents a strong red-shift of −1.12 cm^{-1}. Secondly, the surrounding of the tracks presents a blue-shift like the υ_2 phonon mode, but for this υ_1/υ_3 phonon it is considerably more marked at the bottom apex of all tracks, and with a maximum value of + 0.73 cm^{-1}. This non-symmetric effect between the up and bottom apex of the tracks is not observed in the phonon broadening, but only in its energy shift, and therefore it is not related to lattice defects, but with lattice compressions or dilatations. Also, it can be expected that after the annealing process a large amount of residual stress would be eliminated from the as-fabricated tracks, and therefore these anisotropic lattice changes are some kind of permanent lattice distortion which is accompanied by a refractive index increase along the ***a***-axis (TE modes), and a refractive index decrease for light polarized along the ***c***-axis (TM modes).

#237800 - $15.00 USD Received 10 Apr 2015; revised 22 May 2015; accepted 25 May 2015; published 2 Jun 2015

3.5. Mode simulations and estimation of anisotropic refractive index changes

In order to further understand the refractive index changes we performed a simulation of the waveguide modes with the aim of matching the experimentally observed modes for a given value of the refractive index changes. The elliptical tracks were defined with a fine mesh to dimensions ranging from 11 µm to 16 µm (vertical major axis) and 3 µm (horizontal minor axis), following the obtained track sizes from the Raman mapping analysis. TM and TE modes were studied separately, so as to match the experimental results by varying the unknown refractive index change (Δn) inside the tracks (see section §2.6 for further details). In the first mode analysis, the simulation was run for as many modes as possible (500 modes) around the refractive index of KTP. When the effective index of the desired modes was found, only a reduced number of modes (20) were looked in more detail around the found effective index, so that time consumption could be reduced.

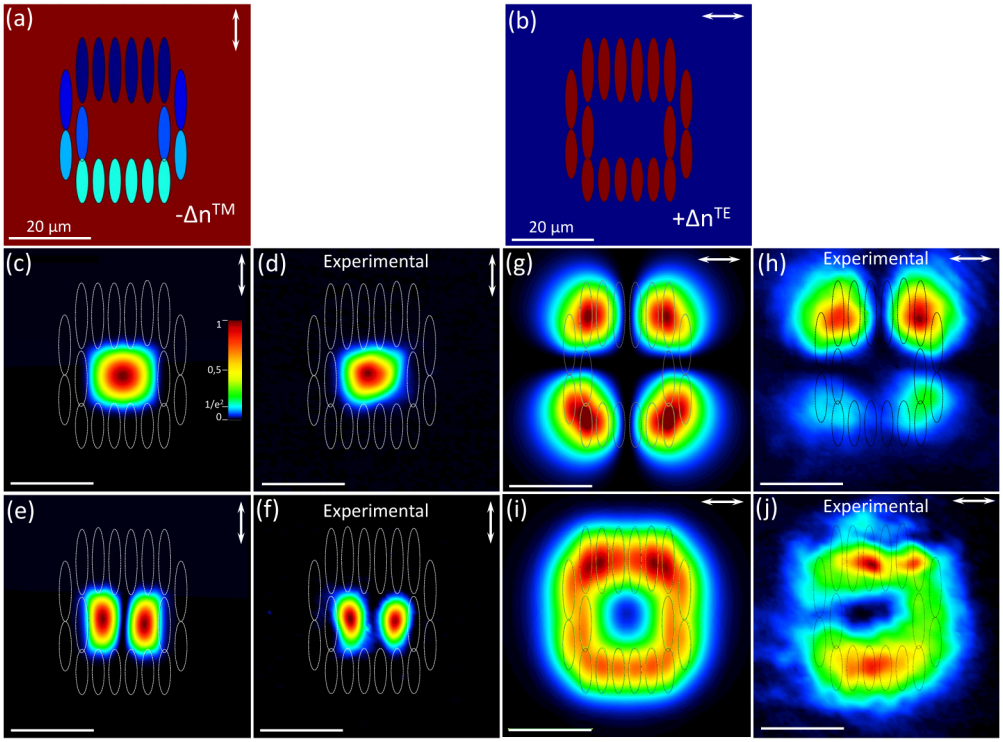

Fig. 8. Results of the simulated modes and experimentally measured ones compared. (a) and (b) show the tracks arrangements. For TM modes an index distribution graded from the upper to lower track rows was used, while for TE modes the best approximation was obtained for a homogenous index change distribution between tracks. Scale bar 20 µm.

For TM modes, due to the non-uniform laser fabrication, it was supposed that the Δn_z^{TM} is not equal for all the tracks. This is also supported by the Raman analysis which shows a stronger lattice distortion in the upper row with respect to the lower row. Therefore, five rows of tracks were applied with different Δn_z^{TM} values, ranging uniformly from 70% to 100% of a maximum Δn_z^{TM}. See Fig. 8(a) for the model followed. After several simulation iterations, it was found that refractive index of the tracks has decreased to a minimum $\Delta n_z^{TM} = -0.01$ in the top 6 tracks, this giving the best match to the experimental modes. Figures 8(c) to 8(f) show the simulated (left) and experimental (right) modes for vertical TM polarization. The light blue color level in the figure depicts the $1/e^2$ intensity level (typically defining the mode field diameter MFD). As it can be seen, for both the fundamental and higher order modes the

#237800 - $15.00 USD Received 10 Apr 2015; revised 22 May 2015; accepted 25 May 2015; published 2 Jun 2015

simulated modes show a very good agreement with the experimental ones. For TE modes, Δn_x was initially also varied in magnitude between upper and lower tracks rows, but this was later disregarded since the complexity of these modes did not allow for such a complex hypothesis and results could not be conclusive. To simplify, the positive Δn^{TE} values were applied to be equal at all the tracks, as schematically shown in Fig. 8(b). From the best matching of the simulated modes with the experimental ones, the Δn_x^{TE} at tracks is found to increase around + 1.5×10^{-3}.

Figures 8(h) and 8(j) show the two basic types of modes experimentally observed for TE polarization. The first mode could be successfully simulated as shown in Fig. 8(g). The observed differences in terms of power spatial distribution between the upper and lower rows are believed to be due to differences between the idealized cladding structure of our model and the real one, as well as to possible scattering losses which could produce an asymmetry in the experimental mode not observable in the ideal simulated model. For the experimental TE mode shown in Fig. 8(j), a combination of various fundamental simulated modes was applied to simulate it. The simulation gave 3 differentiated fundamental modes with power distributions located only in the upper track row, at both lateral sides, or at the lower row (not shown here for the sake of brevity). By overlapping these 3 modes a mode superposition similar to the one observed in the experiment could be obtained (see Fig. 8(i)).

4. Conclusions

In conclusion, we have found that cladding waveguides with good guiding properties for TM (vertical along ***c***-axis) light can be fabricated in KTP crystals and have provided the guidelines for the fabrication of improved structures towards the successful fabrication of Mach-Zehnder optical modulators for 1.55 μm telecom light. We have also shown that an annealing process not only improves the waveguiding quality but also induces an anisotropic refractive index increase at direct laser written tracks of around + 1.5×10^{-3} for TE polarized (a-axis) light. For TM polarized light we have obtained a value of −0.01 for the index decrease at tracks. Moreover, we report that the Raman shift spectra at modified regions (cladding region) is not strongly distorted, and inside the cladding is perfectly un-modified, this allowing to design near-future Mach-Zehnder modulators with good electro-optic coefficients as high as those of the original KTP crystals.

Acknowledgments

This work was partially supported by the Ministerio de Economía y Competitividad, under Project FIS2013-44174-P, by the Spanish Government under project MAT2013-47395-C4-4-R and TEC2014-55948-R and by the Generalitat de Catalunya under project 2014SGR1358. F.D. acknowledges additional support through the ICREA academia award 2010ICREA-02 for excellence in research.

#237800 - $15.00 USD Received 10 Apr 2015; revised 22 May 2015; accepted 25 May 2015; published 2 Jun 2015